Article

Current Biology

Synaptic Connectivity between the Cortex and Claustrum Is Organized into Functional Modules

Graphical Abstract

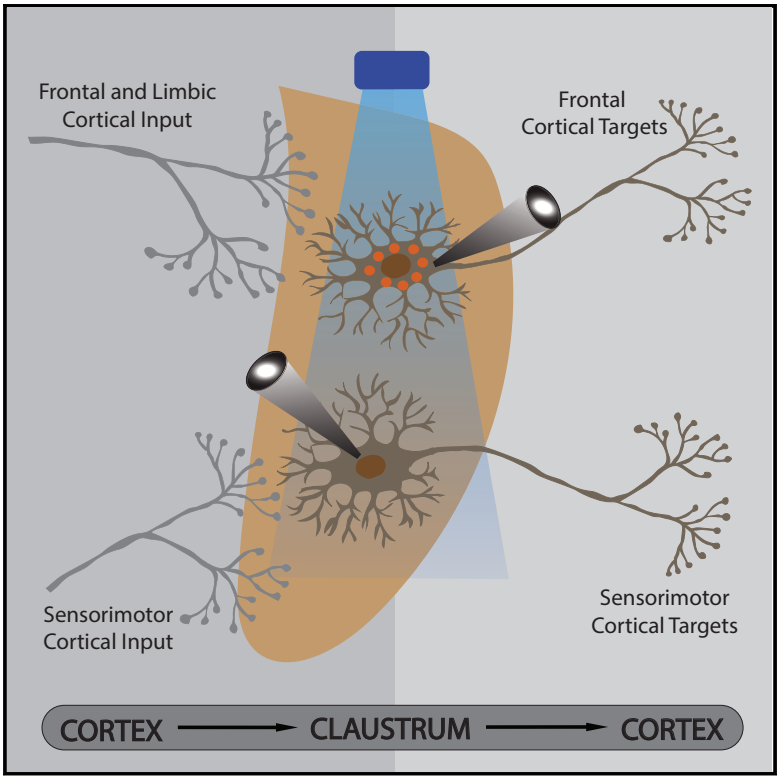

Highlights

- Frontal and limbic cortical regions preferentially target CLA-ACC neurons
- Sensorimotor cortical regions preferentially targeted non CLA-ACC claustrum neurons
- An Insula-CLA-ACC pathway is described, which may underlie the Salience Network
- CLA-ACC neurons mainly co-project to other frontal cortical regions

Authors

Zach Chia, George J. Augustine, Gilad Silberberg

Correspondence

gilad.silberberg@ki.se

In Brief

Using a combination of electrophysiology and anatomical tracing, Chia et al. show that both cortical inputs to and projections from CLA-ACC neurons are highly selective, suggesting that cortico-claustral connectivity is organized as functional modules, specialized in processing different types of information.

Chia et al., 2020, Current Biology *30*, 1–14
July 20, 2020
https://doi.org/10.1016/j.cub.2020.05.031

CellPress

Please cite this article in press as: Chia et al., Synaptic Connectivity between the Cortex and Claustrum Is Organized into Functional Modules, Current Biology (2020), https://doi.org/10.1016/j.cub.2020.05.031

Current Biology

CellPress

Article

Synaptic Connectivity between the Cortex and Claustrum Is Organized into Functional Modules

Zach Chia,[1,2,3] George J. Augustine,[2] and Gilad Silberberg[1,4,*]
[1]Department of Neuroscience, Karolinska Institutet, 17177 Stockholm, Sweden
[2]Lee Kong Chian School of Medicine, Nanyang Technological University, 11 Mandalay Road, Singapore 308232, Singapore
[3]School of Biological Sciences, Nanyang Technological University, 60 Nanyang Drive, Singapore 637551, Singapore
[4]Lead Contact
*Correspondence: gilad.silberberg@ki.se
https://doi.org/10.1016/j.cub.2020.05.031

SUMMARY

The widespread reciprocal connectivity between the claustrum and the neocortex has stimulated numerous hypotheses regarding its function; all of these suggest that the claustrum acts as a hub that connects multiple cortical regions via dense reciprocal synaptic pathways. Although the connectivity between the anterior cingulate cortex (ACC) and the claustrum has been proposed as an important pathway for top-down cognitive control, little is known about the synaptic inputs that drive claustrum cells projecting to the ACC. Here, we used multi-neuron patch clamp recordings, retrograde and anterograde viral labeling, and optogenetics in mouse claustrum to investigate cortical inputs and outputs of ACC-projecting claustrum (CLA-ACC) neurons. Both ipsilateral and contralateral cortical regions were found to provide synaptic input to CLA-ACC neurons. These cortical regions were predominantly frontal and limbic regions and not primary sensorimotor regions. We show that CLA-ACC neurons receive monosynaptic input from the insular cortex, thereby revealing a potential claustrum substrate mediating the Salience Network. In contrast, sensorimotor cortical regions preferentially targeted non CLA-ACC claustrum neurons. Using dual retrograde labeling of claustrum projection neurons, we show selectivity also in the cortical targets of CLA-ACC neurons: whereas CLA-ACC neurons co-projected mainly to other frontal regions, claustrum neurons projecting to primary sensorimotor cortices selectively targeted other sensorimotor regions. Our results show that both cortical inputs to and projections from CLA-ACC neurons are highly selective, suggesting an organization of cortico-claustral connectivity into functional modules that could be specialized for processing different types of information.

INTRODUCTION

The widespread and reciprocal connectivity of the claustrum, a brain region wedged in between the insula and the lateral striatum, has been the impetus behind broad speculation on claustrum function. These functions include consciousness [1], attention [2–4], saliency detection [5–7], and contextual memory [8]. It is assumed that the claustrum acts as a hub that relays inputs between sensory, motor, limbic, and associative cortical regions [1–3, 6]. Various mechanisms for such functions have been proposed. Several studies have suggested cortical integration as the primary mechanism [1, 9–11], while other suggestions include coincidence detection [11], modulation of cortical activity [3], signal amplification [12], and cortical inhibition [4, 13–15]. An underlying requirement of all these suggested mechanisms is that claustrum neurons must receive input from multiple cortical regions and sensory modalities. Previous investigations focusing on multi-modal input to the claustrum have been inconclusive, with some studies suggesting strong sensory integration [16, 17] and others reporting unimodal responses within a multisensory claustrum [5, 18–20]. These divergent results could be related to the specific cortical projections studied. The strongest reciprocal connection across species is between the claustrum and frontal cortical regions such as the anterior cingulate cortex (ACC) [21–25], whereas the connectivity with sensory cortices is sparser [24, 25]. Based on the dense claustrum-ACC connectivity, we hypothesized that CLA-ACC neurons could be a key target of multi-cortical input. The ACC plays an important role in higher cognitive functions [26–28] and is a key node in the Salience Network (SN) [29–36]. We have previously studied CLA-ACC neurons [7] and discovered sexual dimorphism and topological heterogeneity within this population of neurons. Recent work has shown that claustrum neurons projecting to posterior sensory and association cortices receive ACC input [37] and that ACC input to the claustrum plays a role in modulating attentional behavior in rodents [12]. The organizing principles of functional cortical-claustro connectivity, however, remain largely unknown.

Here, we used anterograde viral injections, retrograde bead labeling, optogenetics, and multi-neuron patch clamp recordings to uncover the organization of cortico-claustral synaptic connectivity. We found that CLA-ACC neurons receive monosynaptic inputs from several cortical regions. These inputs were predominantly from frontal and limbic cortices rather than primary sensory and motor regions; specifically, input from the insula forms an insula-claustrum-ACC circuit that can serve as a

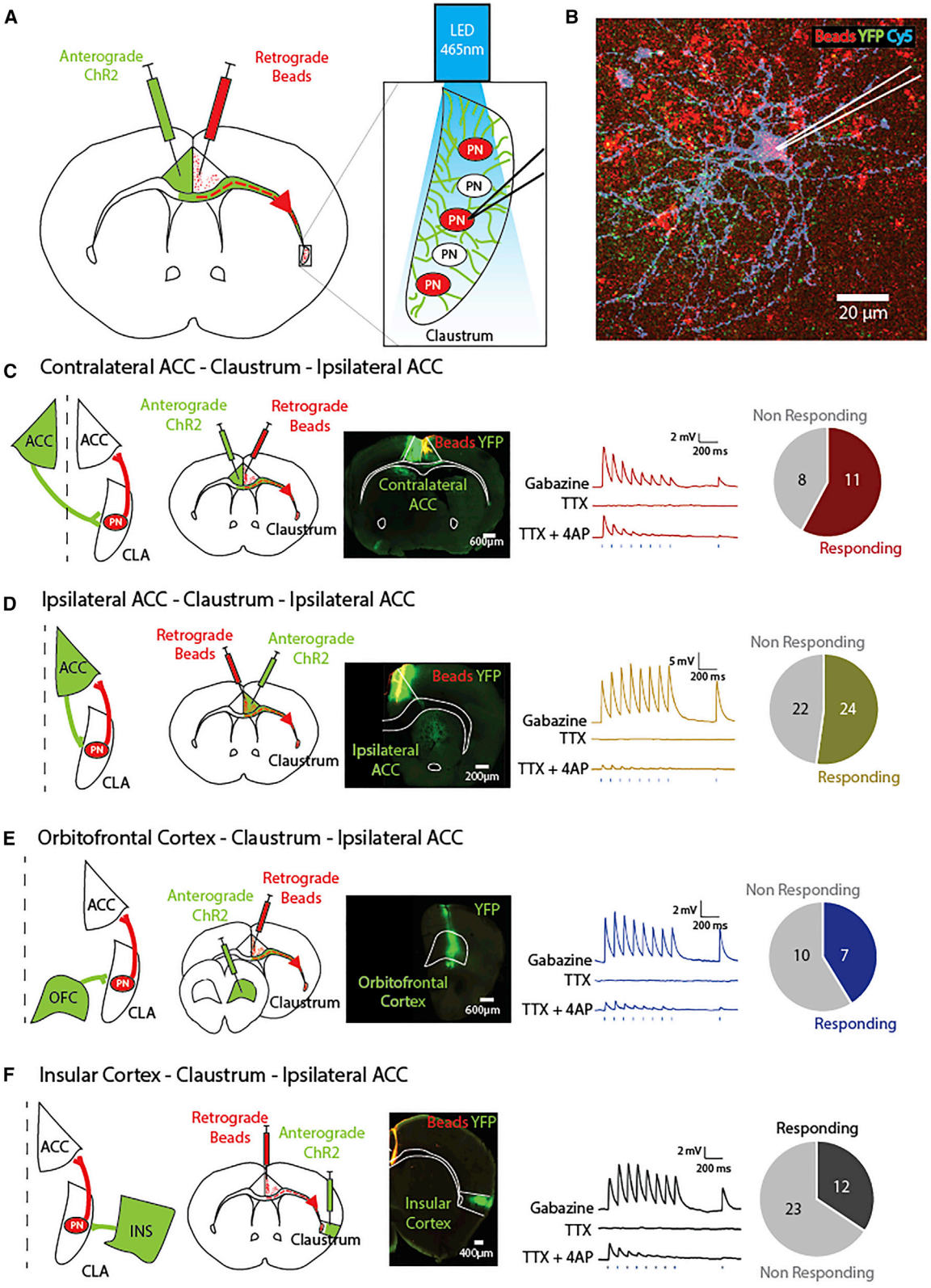

(legend on next page)

Please cite this article in press as: Chia et al., Synaptic Connectivity between the Cortex and Claustrum Is Organized into Functional Modules, Current Biology (2020), https://doi.org/10.1016/j.cub.2020.05.031

substrate underlying the SN. Moreover, we show that claustrum neurons are also selective in their projections to different cortical regions. We showed via dual retrograde bead experiments that claustrum projection neurons have at least two targeting systems – one that targets frontal regions and a second one that targets sensorimotor regions. Our findings support a cortico-claustral organization into functional input and output modules, suggesting that the claustrum operates as a collection of highways rather than a fully convergent hub for cortical inputs.

RESULTS

Robust Frontal-Cortical Input to ACC-Projecting Claustrum Neurons

To characterize cortical input to CLA-ACC neurons, anterograde ChR2 virus driven by a CamKIIa promoter, which preferentially targets glutamatergic cortical projection neurons, was injected into various cortical regions. This enabled photostimulation of synaptic inputs from these regions, while retrograde fluorescent beads were injected into the ACC to specifically label claustrum neurons projecting to the ACC (Figure 1A). As previously shown [7, 24], projections to the ACC mostly arise from the PV-rich claustrum core rather than the claustrum shell or the neighboring insula. Whole-cell patch clamp recordings were made from CLA-ACC neurons identified by fluorescent retrograde beads located in their somata ([Figure 1B; Figure S1], example cells filled with neurobiotin in the patch pipette). The Cortex-CLA-ACC circuit was observed in both male and female mice, and no differences were seen in the respective postsynaptic responses (Table S1).

We first asked whether frontal cortical regions provide input to CLA-ACC neurons. The three cortical areas considered were the contralateral ACC (Figure 1C), ipsilateral ACC (Figure 1D), and ipsilateral orbitofrontal cortex (OFC, Figure 1E). Postsynaptic responses were observed in bead-labeled CLA-ACC neurons in response to photostimulation of axons from all three frontal cortices: contralateral ACC (11 responding cells in 19 recordings, n = 3 mice, Figure 1C), ipsilateral ACC (24/46, n = 6 mice, Figure 1D), and OFC (7/17, n = 3 mice, Figure 1E). In a subset of these three robust connections, additional pharmacological procedures were used to determine whether the connections were excitatory and monosynaptic [38]. Postsynaptic responses were obtained in the presence of the $GABA_A$ receptor antagonist gabazine (10 μM) and were blocked following application of NBQX (10 μM) and APV (50 μM, Figure S2A, n = 4 neurons). EPSPs were abolished upon bath application of Tetrodotoxin (TTX, 1 μM; Figure 1C–1E), indicating that responses were synaptic and not caused by direct photostimulation of claustrum neurons. Subsequent bath application of 4AP (100 μM) restored postsynaptic responses to inputs from contralateral ACC (2/4 neurons; Figure 1C), ipsilateral ACC inputs (4/16 neurons; Figure 1D) and OFC (3/4 neurons; Figure 1E) indicating that the connection from cortex to CLA-ACC cell was monosynaptic and that disynaptic contralateral ACC-CLA-ACC and OFC-CLA-ACC circuits exist. Responses to photostimulation of axons from different presynaptic cortical regions differed in their short-term plasticity (Figure 1). Responses from contralateral ACC displayed stronger depression and lower paired-pulse ratios (PPR) than the ipsilateral responses (Figure S2B). Future experiments using opsins with faster kinetics [39, 40] are required to systematically investigate the synaptic dynamics of cortical-claustrum inputs at a wider frequency range.

Monosynaptic Projections from Insula to ACC-Projecting Claustrum Neurons

Whereas the insula and ACC are functionally correlated [29–32] they are not structurally connected [7, 22, 24]; conversely, retrograde labeling shows that there is strong claustrum-ACC projection. We previously suggested that these regions may be connected via the claustrum in an insula-claustrum-ACC circuit [7]. Recent anatomical studies reported that axon terminals or passing fibers were observed passing from the insula to the claustrum [41, 42]. To directly determine whether the insula provides input to CLA-ACC neurons, anterograde ChR2 virus was injected into the insula, while retrograde fluorescent beads again were injected into the ACC (Figure 1F). To ensure that injected virus did not extend into the claustrum, we used smaller injection volumes, faster injection rates, and shorter waiting times (Table 1). Postsynaptic responses were recorded in CLA-ACC neurons in response to photostimulation of insula-claustrum projections (12/35 neurons, n = 9 mice). Responses were abolished upon bath application of TTX and were restored by addition of 4AP (5/6 neurons), thus indicating monosynaptic connection (Figure 1F). These results show that, despite the sparsity of direct projections from the insula to ACC, a synaptic insula-claustrum-ACC pathway exists via disynaptic excitatory connections from insula to claustrum and claustrum to ACC. Previous studies using various methods have shown that projections to the ACC arise mainly from the claustrum core rather than the claustrum shell or insula [7, 24, 43, 44]. To verify this point we injected retrograde viral tracer in the ACC of two PV-tdTomato mice and imaged the PV-defined claustrum core. Cell bodies and neurites of retrogradely labeled, claustrum-projecting ACC neurons were

Figure 1. ACC-Projecting Claustrum Neurons Receive Robust Input from Frontal Cortical Sites

(A) Illustration of the experimental paradigm for studying multi-cortical input to CLA-ACC neurons. Red retrograde fluorescent beads were injected into the ACC, and AAV-mediated ChR2 virus was injected into the tested afferent cortical region. After at least 20 days of post-surgery recovery, mice were sacrificed and whole-cell patch clamp recordings performed on bead-labeled claustrum neurons.

(B) Example of a bead-labeled claustrum neuron following neurobiotin staining via the patch-clamp pipette.

(C–E) Illustration of the experimental paradigm studying contralateral ACC, ipsilateral ACC, and ipsilateral OFC inputs to CLA-ACC neurons. Map of injection sites based on the Paxinos and Franklin Mouse Atlas (left) and the corresponding confocal image of 250 μm coronal slice with ChR2 injected into the cortical region (center). Example of responses of CLA-ACC neurons to input from (C) contralateral ACC (11/19 neurons), (D) ipsilateral ACC (24/46 neurons), and (E) ipsilateral OFC (7/17 neurons), respectively. Postsynaptic response to photostimulation was abolished with bath application of TTX and recovered upon 4AP application. The pie chart (right) shows the numbers of responding and non-responding CLA-ACC neurons to axonal projections from the various cortices. (F) CLA-ACC neuron receiving insular input (12/35 neurons). Postsynaptic response to photostimulation was abolished in 5/6 instances with bath application of TTX and recovered upon 4AP application. Abbreviations as follows: ACC, anterior cingulate cortex; OFC, orbitofrontal cortex; INS, insula; CLA, claustrum.

See also Figure S1, Figure S2, Figure S3, and Table S1.

Table 1. ChR2 Injection Parameters

Cortical Site	Injection Volume (nl)	Injection Rate (nL/min)	Diffusion Time (min)	L-M	A-P	D-V	Number of mice	Number of mice with no responding neurons	Average Age at Operation/ Experiment
Orbitofrontal Cortex	300	100	5	−1	2.5	−2.5	3	0	P60/ 83
Contralateral ACC	300	100	5	0.2	0.7	−1.4	3	0	P47/ 74
Ipsilateral ACC	300	100	5	−0.2	0.7	−1.4	6	0	P57/ 86
Insula	100	200	3	−3.6	0.7	−4.3	9	3	P52/ 81
Contralateral Motor Cortex	400	100	5	1.4	0.7	−1.5	3	2	P45/ 75
Somatosensory Cortex	400	100	5	−2.9	0.6	−2.2	3	3	P48/ 80
Visual Cortex	400	100	5	−2.4	−2.4	−0.9	3	2	P55/ 90
Auditory Cortex	400	100	5	−3.9	−2.8	−2.5	3	3	P57/ 83

labeled in the PV-defined claustrum core and shell areas but not in the insula (Figure S3).

Weak Sensorimotor-Cortical Input to ACC-Projecting Claustrum Neurons

To determine whether primary sensorimotor regions also provide similarly robust input to CLA-ACC neurons, we used the same experimental paradigm to analyze input from four sensory cortical regions: visual cortex (Figure 2A), contralateral motor cortex (Figure 2B), auditory cortex (Figure 2C), and somatosensory cortex (Figure 2D). The ipsilateral motor cortex was not considered because it is known that projections from the motor cortex to the claustrum primarily arise from the contralateral hemisphere [20, 25]. Light-evoked postsynaptic responses were rarely recorded in response to photostimulation of axons from the visual cortex (1/25 recordings, n = 3 mice, Figure 2A) or the contralateral motor cortex (2/29, n = 3 mice, Figure 2B). Further, no CLA-ACC neurons responded to photostimulation of the auditory cortex (0/19, n = 3 mice, Figure 2C) or somatosensory cortex (0/37, n = 3 mice, Figure 2D). These results show that CLA-ACC neurons receive minimal input from primary sensorimotor cortices. To determine whether sensorimotor projections target non CLA-ACC neurons, we used the same experimental paradigm to analyze input from a combination of sensorimotor regions to non-CLA-ACC neurons. To that end, ipsilateral visual and auditory cortices (n = 3 mice) as well as somatosensory and contralateral motor cortices (n = 2) were virally transduced with ChR2. Red retrograde beads were injected into the ACC in the same method described above (Figure S2C). In stark contrast to the lack of response in CLA-ACC neurons, photostimulation induced synaptic responses in claustral neurons that did not contain retrobeads, namely non-CLA-ACC neurons (11/35, Figure 2E). These results collectively suggest that sensorimotor projections target non CLA-ACC neurons preferentially over CLA-ACC neurons.

Selective Cortical Inputs to ACC-Projecting Claustrum Neurons

Our data permitted comparison of the inputs provided to the claustrum by numerous cortical regions (Figure 3A). The fraction of CLA-ACC neurons receiving frontal cortical input was 51.2% (42/82 neurons) compared to 2.7% (3/110) from sensorimotor areas and 34.3% (12/35) from the insula, a limbic area (Figure 3A-B, $p < 0.001$, Chi-square test). These results indicate a significant bias in claustrum inputs from frontal and limbic cortices. In regard to the physiological properties of the excitatory input to CLA-ACC neurons, there were no significant differences in onset latencies or EPSP amplitudes between responses to photostimulation of inputs from all cortical areas ($p > 0.4$, one-way ANOVA; Figure 3C-D). We previously revealed topological heterogeneity in the distribution of CLA-ACC neurons based on their intrinsic properties [7], suggesting a rostro-caudal topographic organization within the claustrum. To investigate the relationship between the location of the neurons within the claustrum and their cortical input we subdivided CLA-ACC neurons into the previously described anterior, middle, and posterior claustrum regions. Frontal cortical projections targeted CLA-ACC neurons in the anterior and middle claustrum, ($p < 0.001$, chi-square test, Figure 3E), and the small number of sensorimotor cortical projections which targeted ($p < 0.001$, Fishers Exact test, Figure 3E) CLA-ACC neurons were found in the anterior claustrum. Insula input did not show a preference for any part of the claustrum ($p > 0.05$, chi-square test, Figure 3E). These results suggest that CLA-ACC neurons preferentially receive input from frontal and limbic input rather than sensorimotor cortical input. Further, these neurons are not homogeneously distributed within the claustrum.

Insula Targets PV- and Non-PV-Expressing Claustrum Neurons

We showed above that insula provides excitation to CLA-ACC neurons (Figure 1F). We next detailed the projections and recipient neurons of the insula-claustrum pathway. To determine the structural relationship between the claustrum and projections from the insula, we used PV-tdTomato transgenic mice (Figure 4A). These mice enabled visual determination of the claustrum core region, which is enriched in PV-expressing interneurons and their processes [45, 46]. To visualize insula inputs to the claustrum, ChR2 was virally transduced in the insula of these mice. Using this strategy, we found that projections from the insula targeted the ipsilateral but not contralateral claustrum (Figure 4B1; Figure S4, for additional examples of insula injections). This arrangement was further documented by photostimulating the ChR2-expressing insula axons while recording from claustrum neurons. No postsynaptic responses were ever observed in the contralateral claustrum (0/24 recordings, n = 7 mice,

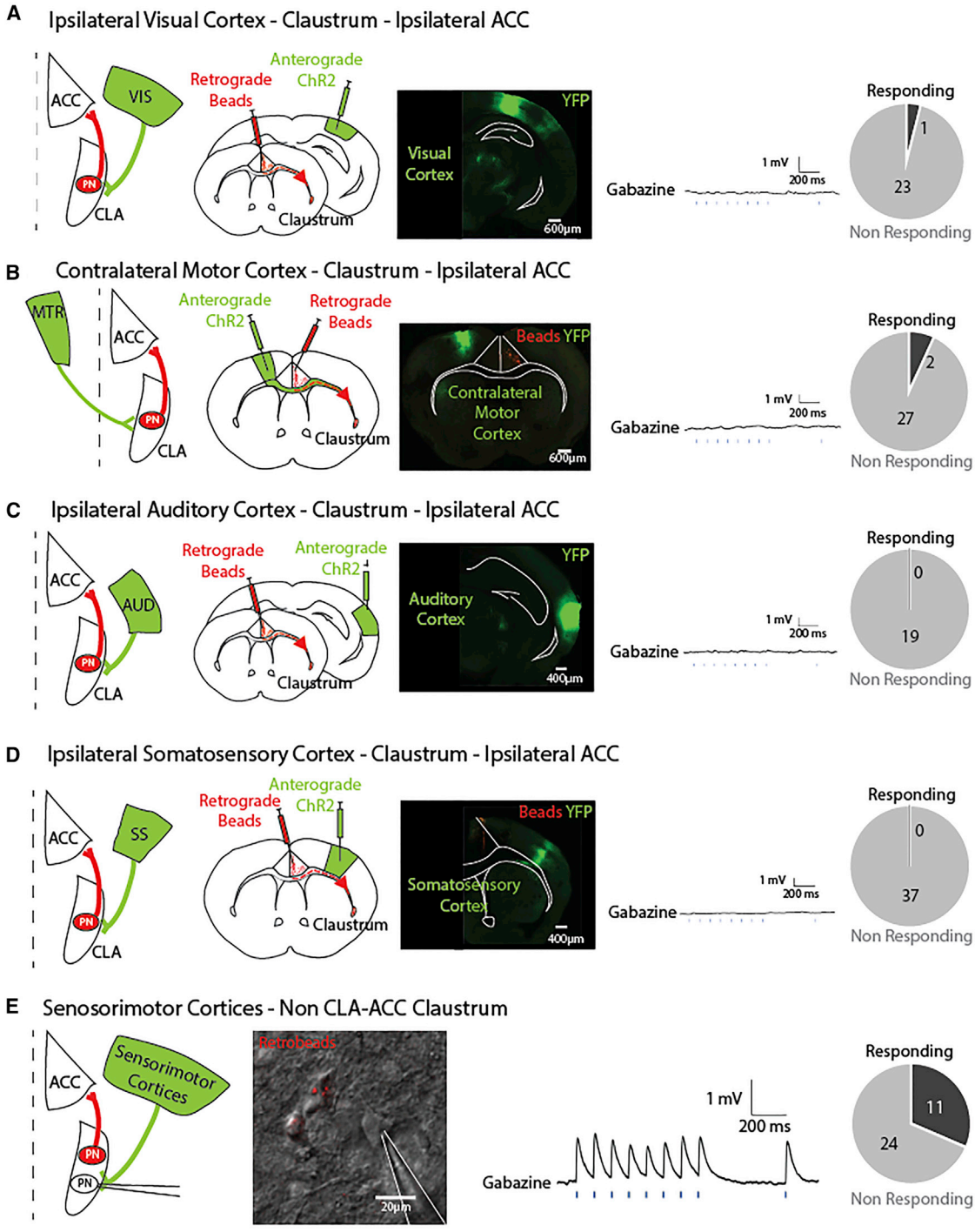

Figure 2. ACC-Projecting Claustrum Neurons Receive Weak Input from Sensorimotor Cortices

Illustration of the experimental paradigm studying inputs to CLA-ACC neurons originating from (A) visual cortex, (B) contralateral motor cortex, (C) auditory cortex input, and (D) somatosensory cortex. Map of injection sites based on the atlas and corresponding confocal image of 250 µm experimental slice with ChR2 injected into the cortical region to the right of the experimental paradigm. (A) Visual (1/25 neurons), and (B) contralateral motor cortices (2/29 neurons) were found to send input to CLA-ACC neurons. No CLA-ACC neurons were found to respond to (C) auditory (0/19 neurons) and (D) somatosensory (0/37 neurons) cortex axons. Example traces reflect the commonly observed non-responding outcome. Pie chart (right) shows the number of responding and non-responding CLA-ACC neurons to axonal projections from the various cortices. (E) Sensorimotor input was found to project to non CLA-ACC neurons at a higher probability (11/35 neurons). Abbreviations as follows: MTR, contralateral motor cortex; SS, somatosensory cortex; VIS visual cortex; AUD, auditory cortex; CLA, claustrum. See also Figure S2.

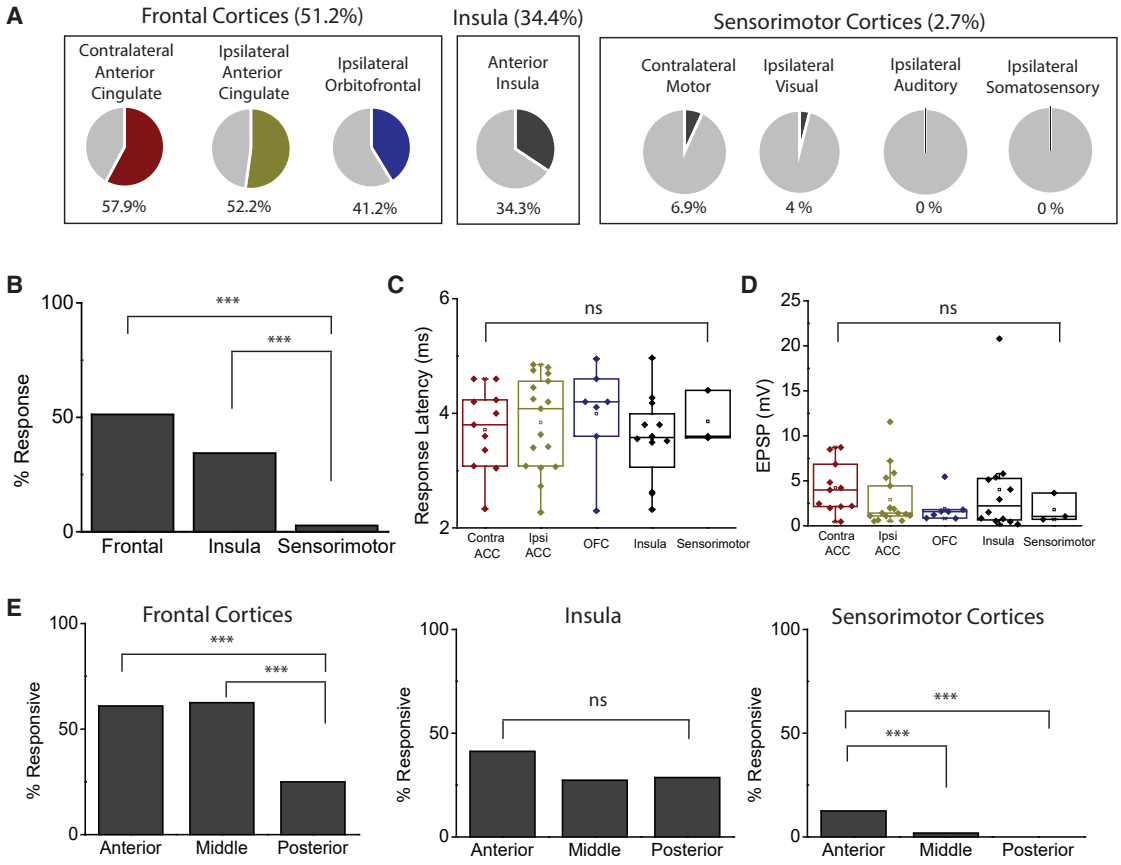

Figure 3. Cortical Input to ACC-Projecting Claustrum Neurons Is Biased to Frontal and Limbic Regions Rather than Primary Sensorimotor Regions

(A) Response rates for each cortical input condition.

(B) Histogram of response rates of frontal regions (contralateral ACC, ipsilateral ACC, OFC (42/82 neurons) and limbic region/insula cortex (12/35 neurons) were significantly higher than sensory regions (visual, cortex, auditory cortex, somatosensory cortex, contralateral motor cortex (Right). 3/110 neurons, $p < 0.001$, chi-square test). There was no difference between rate of response of frontal and limbic cortices ($p > 0.05$, chi-square test).

(C) Response Latency and (D) EPSP size were similar across all three regional inputs ($p > 0.05$, one-way ANOVA).

(E) Topological response profiles of responding CLA-ACC neurons. Frontal cortex projecting axons preferentially targeted anterior and middle CLA-ACC neurons ($p < 0.001$, chi-square test); no topographical preference was observed for insular cortex and sensorimotor cortical projections ($p > 0.05$, chi-square test).

Figure 4C). At higher magnification, neurites could be observed emerging from layer 5, rather than layer 2/3, of the ipsilateral insula (Figure 4B2), suggesting that projections originated at layer 5 of the insula. This was consistent with a lack of postsynaptic responses in claustrum neurons when photostimulating insula axons following injection of ChR2 virus selectively into layer 2/3 of the insula (0/24, n = 5 mice, Figure 4C). This contrasts with the postsynaptic response rate in the ipsilateral claustrum to photostimulation of insula layer 5 (Figure 4C). In a subset of these connections we also determined whether connections were monosynaptic (Figure 4D). PSPs were abolished following bath application of TTX and were restored when 4AP was added, indicating that insula input to the claustrum is monosynaptic (n = 11 neurons, Figure 4D). Postsynaptic responses were abolished by bath application of the glutamate receptor blockers NBQX (10 μM) and APV (50 μM), indicating that the insula input to the claustrum was excitatory (n = 12 neurons, Figure 4D). Together, this shows that the layer 5 of insula provides monosynaptic excitatory input to the claustrum.

Having established that claustrum projection neurons receive monosynaptic excitatory input from the insula (Figure 1F), we next asked whether PV-expressing interneurons also received such input. To directly compare insula synaptic inputs, we obtained recordings from fluorescently labeled PV interneurons and neighboring non-PV neurons within the claustrum (Figure 4E). In a subset of experiments, paired recordings were obtained, enabling direct comparison of synaptic properties under the same experimental conditions with regard to viral transduction and optogenetic photostimulation. Non-PV neurons were classified based on their intrinsic electrical properties and action potential waveforms and were observed to be of the strongly adapting or mildly adapting types previously observed in claustrum projection neurons [7]. Both types were observed to receive synaptic input from the insula and there were no differences in their postsynaptic responses to insula photostimulation (Figure S5); thus, these responses were pooled in subsequent analyses. We found that both PV and non-PV neurons receive synaptic input from the insula (Figure 4E). There was no difference

Please cite this article in press as: Chia et al., Synaptic Connectivity between the Cortex and Claustrum Is Organized into Functional Modules, Current Biology (2020), https://doi.org/10.1016/j.cub.2020.05.031

CellPress

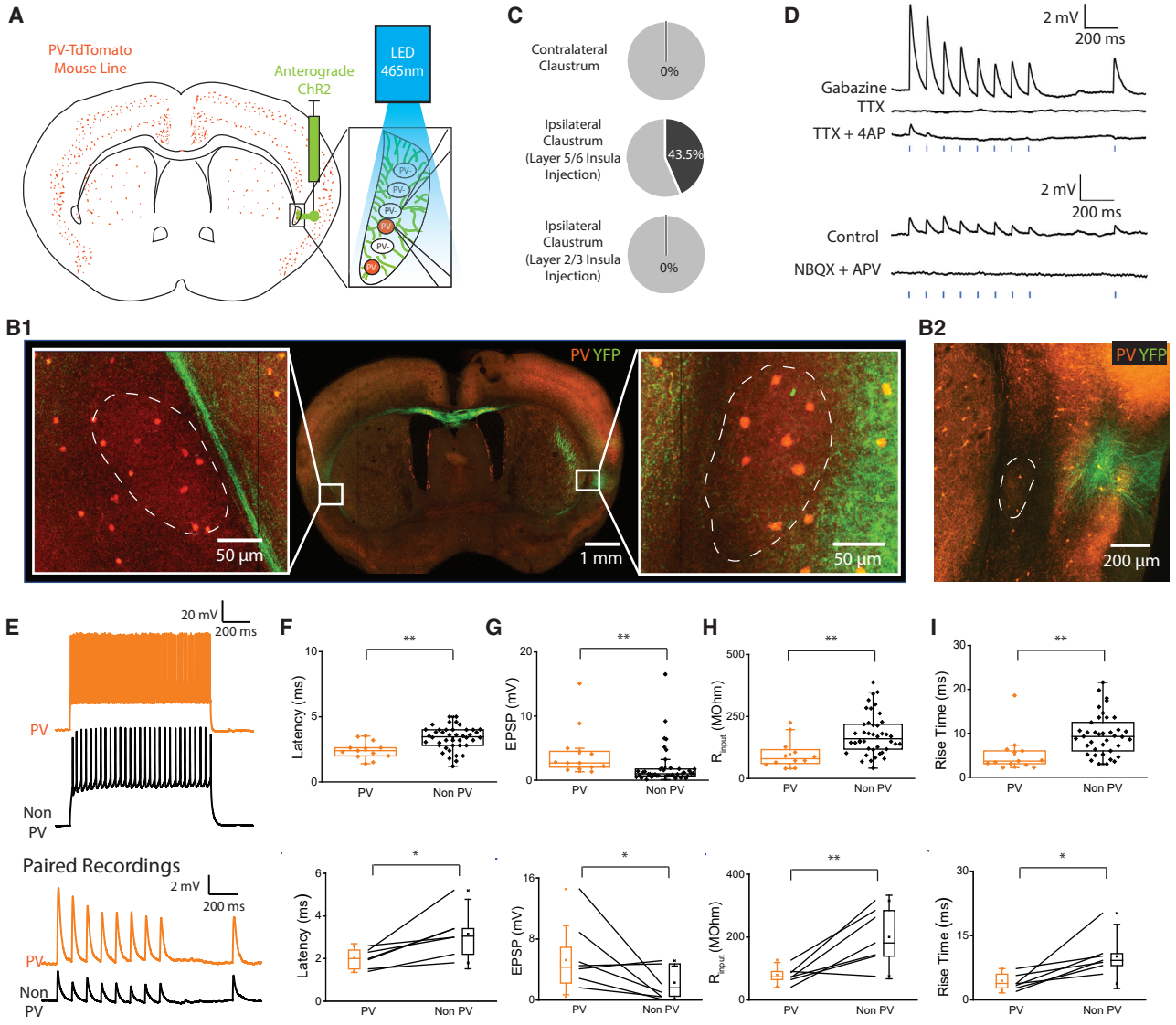

Figure 4. Insular Projections Target both PV and non-PV Neurons in the Claustrum

(A) Illustration of the experimental paradigm. Briefly, ChR2 was injected using an anterograde viral vector into the insula (100 nl, 200 nL/min). PV-tdTomato transgenic mice were used to enable unambiguous identification of the claustrum. Mice were sacrificed for experiments after at least 20 days of recovery. Whole-cell patch clamp recordings of claustrum cells and whole field illumination was made to test for postsynaptic response to photostimulation.

(B1) Confocal image of a 250 µm thick slice, showing injection into layer 5 of insula without spillage into claustrum core and shell regions (31 out of 103 injected mice had acceptable injections for these experiments). Close-up into the claustrum identified by PV-rich a region shows YFP-expressing fibers in ipsilateral claustrum (Right) but not contralateral claustrum (Left).

(B2) Image of injection into layer 2/3 of the insula shows that projections are confined within layer 2/3 and do not reach into the claustrum.

(C) Postsynaptic responses were recorded in the ipsilateral claustrum (65/161 recordings, 0/24 in contralateral claustrum) from layer 5 insula projections only (0/24 responses in claustrum after layer 2/3 insula injection).

(D) A subset of recordings was further tested for verifying the existence monosynaptic connections (n = 11). Synaptic responses to photostimulation were abolished following bath application of TTX and recovered upon additional 4AP bath application. Another subset of recordings was tested for excitatory connections (n = 12) via the use NBQX and APV which abolished the postsynaptic response to photostimulation.

(E) Both PV and non-PV neurons received input from the insula. Top: voltage responses to suprathreshold step current injections. Bottom: examples of synaptic responses of simultaneously recorded PV and non-PV neurons to photostimulation of synaptic terminals.

(F–I) Properties of synaptic responses in PV and non-PV neurons to photostimulation of terminals from insula (Top). The same properties were extracted from simultaneous (paired) recordings PV and non-PV neurons (Bottom). Whiskers represent 25-75 percentile ± SD

(F) Latency of response from photostimulation shows that PV cells respond with shorter latency compared to non-PV neurons ($p < 0.01$, t test), this difference in onset latency is observed also in paired recordings ($p < 0.01$, paired t test).

(G) EPSP size from photostimulation shows that PV cells have larger EPSP size compared to non-PV neurons ($p < 0.01$, t test); This same difference in EPSP size is also observed in paired recordings ($p < 0.05$, paired t test).

(legend continued on next page)

in the probability for obtaining light-evoked responses between PV and non-PV neurons (65/161 neurons in 31 mice, in which 13/26 are PV interneurons, $p > 0.05$, chi-square test).

The onset latency of synaptic responses was shorter for PV interneurons than for non-PV neurons (Figure 4F, n = 42 non-PV neurons 3.48 ± 0.1 ms SEM, n = 12 PV interneurons 2.43 ± 0.2 ms SEM; $p < 0.001$, t test). This was confirmed in paired recordings from PV and neighboring non-PV neurons (Figure 4F, n = 7 pairs, projection neurons 3.15 ± 0.41 ms SEM, PV interneurons 2.02 ± 0.17 ms SEM; $p < 0.01$, single-tail paired t test). Synaptic responses were significantly larger in PV interneurons (Figure 4G, n = 42 non-PV neurons 1.07 ± 0.46 mV SEM, n = 12 PV interneurons 4.28 ± 1.11 SEM; $p < 0.01$, t test; n = 7 pairs, non-PV neurons 2.01 ± 0.8 mV SEM, PV interneurons 5.91 ± 1.7 mV SEM $p < 0.05$, single-tail paired t test). In agreement with previously published data [12, 46], PV cells had a lower input resistance compared to non-PV neurons (Figure 4H, n = 42 projection neurons 158 ± 13 MOhm SEM, n = 12 PV interneurons 98 ± 17 MOhm SEM; $p < 0.01$, t test; n = 7 pairs, non-PV neurons 200 ± 34 MOhm SEM, PV interneurons 79 ± 10 MOhm; $p < 0.01$, single-tail paired t test). This indicates that the observed differences in EPSP amplitude were not simply due to differences in neuronal input resistance, which would amplify EPSPs in non-PV neurons. The rise time of EPSPs in PV cells was significantly shorter than in non-PV neurons (Figure 4I, n = 42 non-PV neurons 11.5 ± 0.7 ms SEM, n = 12 PV interneurons 5.4 ± 1.3 ms SEM; $p < 0.001$, t test; n = 7 pairs, projection neurons 10.1 ± 1.9 ms SEM, PV interneurons 4.5 ± 0.7 ms; $p < 0.05$, single-tail paired t test), providing another indication that PV interneurons respond to insula input faster and with larger EPSPs compared to neighboring non-PV neurons. In summary, our data support the existence of both a monosynaptic excitatory and a feedforward inhibitory pathway within the insula-claustrum projection, as previously proposed for other cortico-claustrum afferent pathways [46].

Selective Output of ACC-Projecting Claustrum Neurons

A single claustrum neuron can project to more than one cortical area and hemisphere [20, 47–50]. The selectivity in cortical inputs to CLA-ACC neurons raised the question of whether CLA-ACC neurons were similarly selective in their projection to other cortical targets. To determine whether CLA-ACC neurons co-project to other cortices, red retrograde fluorescent beads were injected into the ACC, while green fluorescent beads were injected into another cortex (Figure 5A). Retrograde fluorescent beads were chosen as a tracer due to their low false positive rates, low toxicity in animals and high stability over time [51–53]. Red fluorescent beads were used to identify CLA-ACC neurons as well as identify the claustrum region [7], whereas green beads identified claustrum projections to the second target cortex. A claustrum neuron had at least two cortical targets if its soma showed co-labeling of both red and green beads (Figure 5B). A total of six cortical targets were tested for co-projection with CLA-ACC neurons: Retrosplenial Cortex (RSP) Orbitofrontal Cortex (OFC), Visual Cortex (VIS) Motor Cortex (MTR), Auditory (AUD), and Somatosensory (SS, Figure 5C; Figure S6). To calculate the degree of co-localization, the number of co-labeled cells was divided by the total number of green-labeled cells. Co-projection of CLA-ACC neurons with other frontal and limbic regions (RSP, 53%; OFC, 45%) was several-fold higher than co-projection to sensorimotor regions (VIS, 15%; MTR, 13%; AUD, 13%; SS, 10%; Figure 5D, $p < 0.001$, chi-square test). There was no significant difference in the co-labeling of CLA-ACC neurons with RSP and OFC ($p > 0.1$, chi-square test) and there was no significant difference in the co-labeling rates of CLA-ACC neurons with the sensorimotor regions ($p > 0.1$, chi-square test; see the second table in Method Details).

To identify the target preference of sensorimotor-projecting claustrum neurons, we injected red and green retrograde beads into different sensorimotor cortical regions (AUD, VIS, SS or MTR, Figure 5C). Roughly one third of labeled cells co-projected to other sensorimotor regions ($p > 0.1$, chi-square test, Figure 5E). This fraction was threefold higher than that of sensorimotor cells projecting to the ACC (Figure 5F, $p < 0.001$, chi-square test), however, it was significantly lower than the fraction of CLA-ACC neurons co-projecting to frontal regions (Figure 5F, $p < 0.001$, chi-square test).

In summary, our data show that CLA-ACC neurons strongly interact with frontal and limbic cortical areas with sparser interactions with sensorimotor ones, whereas sensorimotor regions are targeted by a different claustral population. Thus, claustrum projection neurons display preferences in their synaptic projection targets, suggesting a modular organization for claustro-cortical interconnectivity (Figure 6).

DISCUSSION

Multi-cortical input to the claustrum is an important requirement that underpins all current hypotheses regarding claustrum function. In this study we investigated whether CLA-ACC neurons receive and provide multi-cortical input. Our experiments identified six cortical regions that provide monosynaptic input to CLA-ACC neurons, with input from frontal and limbic cortical regions being more prominent than that from primary sensory and motor regions. Target preference was also seen in the projections from claustrum to different cortical regions. These inputs are summarized in Figure 6. We also established an insula-claustrum-ACC pathway that may serve as part of the SN and found that insula projections to the claustrum target both projection neurons and PV interneurons, with stronger input to the latter.

Strengths and Limitations of Our Experimental Methods

To investigate multi-cortical input to the claustrum we used a double injection protocol: retrograde fluorescent beads into

(H) Input resistance size of PV cells is smaller than non-PV neurons ($p < 0.01$, t test); this difference in input resistance is observed also in paired recordings ($p < 0.05$, paired t test).

(I) The rise time of the response neurons is faster in PV cells compared to non-PV neurons ($p < 0.05$, t test), this difference in rise time is observed also in paired recordings ($p < 0.05$, paired t test). Response rates of PV and non-PV neurons in ipsilateral claustrum are comparable ($p > 0.05$, chi-square test, not shown). See Figure S4 and Figure S5.

Please cite this article in press as: Chia et al., Synaptic Connectivity between the Cortex and Claustrum Is Organized into Functional Modules, Current Biology (2020), https://doi.org/10.1016/j.cub.2020.05.031

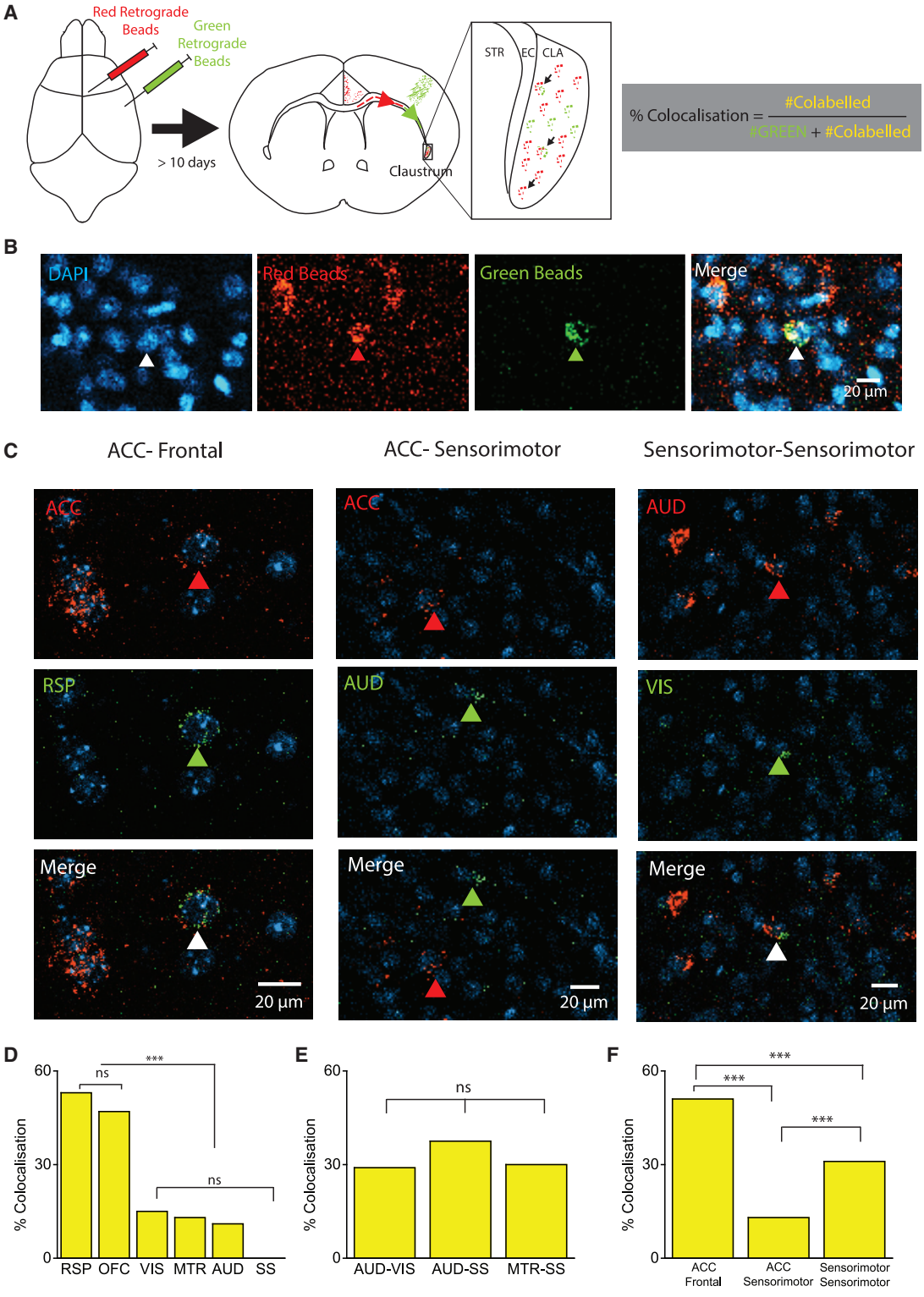

Figure 5. CLA-ACC Neurons Co-project to Frontal Cortical Areas Rather than Sensorimotor Areas

(A) 41 C56/B7J mice were injected with two colors of retrograde fluorescent beads. Red retrograde beads were injected into the ACC and green retrograde beads were injected into another cortex. Mice were sacrificed after 10 days. Brains were cryosectioned and images were taken to identify neurons co-labelled for red and green beads and counted.

(B) Example of red and green beads co-labelled cells with nuclear-stain DAPI.

(legend continued on next page)

the ACC, paired with anterograde ChR2 virus into various cortical regions. The double injection protocol enabled unambiguous identification of CLA-ACC neurons and the isolation of projections from specific cortical regions, thus revealing disynaptic links between these cortical regions and the ACC mediated by claustrum neurons. Neurons targeting other regions were not studied and are therefore open for further investigation. In a subset of experiments studying insula input to the claustrum, we used dual patch clamp recordings to compare the afferent input to neighboring neurons of different types. This approach allowed us to study these inputs under identical experimental conditions, in regard to viral injection, mouse age, and precise topographic location. There are limitations to our experimental design that should be noted. Despite attempting to maximize viral transduction within the cortex, this does not guarantee that every projection neuron within the injected region expressed ChR2. To minimize feedforward polysynaptic activity, the light source used for photostimulation was set at intensities that were sufficient to generate EPSPs but not action potentials in the postsynaptic cell (see STAR Methods). Hence, while response probability indicates the relative bias of CLA-ACC neurons to different cortical inputs, a lack of observed response does not completely eliminate the possible existence of a connection from a given cortical region. To investigate multi-cortical input to the claustrum we used a double injection protocol: retrograde fluorescent beads into the ACC, paired with retrograde fluorescent beads of a second wavelength into another cortical region. This dual injection protocol took advantage of the robust CLA-ACC pathway to enable unambiguous identification of CLA-ACC neurons and the claustrum region in wild type mice and revealed the presence of co-projecting claustrum neurons that target the frontal areas. Despite the advantages of retrograde fluorescent beads (stability, low toxicity, low false positive rate), green beads are weaker in uptake and fluorescence compared to red beads, a known supplier limitation that can be minimized by using young animals (less than 2 months). Therefore, it is likely that our measured numbers of co-projecting neurons may be an underestimate.

Multi-cortical Input to ACC-Projecting Claustrum Neurons

We found that CLA-ACC neurons receive cortical input from the contralateral and ipsilateral ACC, OFC, insula, contralateral motor cortex, and visual cortex. We did not observe cortical input to these neurons from the somatosensory or auditory cortices. Pharmacological analyses established that the contralateral ACC, OFC, and insula form disynaptic connections with the ACC through claustrum neurons, whereas the ipsilateral ACC forms a reciprocal excitatory pathway with claustrum via a weak monosynaptic connection. We observed a difference in connection probability with frontal (ACC, OFC) and limbic cortices (insula) more likely to synapse on CLA-ACC cells, whereas the input from sensorimotor cortices is much less common (contralateral motor cortex, visual cortex) or not found (ipsilateral somatosensory cortex, auditory cortex). Additionally, we observed that sensorimotor cortical neurons target non-ACC projecting claustrum neurons suggesting a modular organization. Recent work by Zingg and colleagues [44] suggests that claustrum neurons projecting to the retrosplenial cortex receive only sparse innervation from primary sensory cortical regions. The PPRs observed in Figure S2 suggest that inputs from different cortical regions may have different presynaptic release probabilities, which could have different effects on downstream activity of the claustrum [54]; further work will be required to define the properties of presynaptic terminals in the cortico-claustral circuit. Our results do not address whether multi-cortical input arises only at the population level or is also seen at the level of individual neurons; this question is highly relevant for future investigation.

Evidence for a Possible Substrate for the Salience Network

We have defined a monosynaptic insula-claustrum-ACC circuit which potentially underlies the SN. SN integrity has been negatively correlated with executive control in alcohol abuse disorders [55] and SN dysfunction has been implicated in schizophrenia [56–58] among other psychological disorders. The SN switches brain state activity from the Default Mode Network to Central Executive Network and is activated in response to salient events. The main nodes for this network activity are the insula and ACC [29–36]. The paucity of ACC-projecting insula cells [7, 24, 44], distinction in anatomical projections between insula and claustrum [59], and joint consideration of insula and claustrum in SN studies [29, 60–63] together raise the possibility that the claustrum plays a key role in the SN [6, 7, 43]. The particular role of the claustrum in the SN - whether as a link between the insula and ACC or as a main node of the salience network instead of the insula - is a question to be clarified in future work [43].

Insula-Claustrum Circuits Suggest a General Claustrum Response to Cortical Input

Studying the insula-claustrum circuit is technically challenging due to the proximity of these two regions [24, 25, 44]. We circumvented this challenge via focal injection of ChR2-expressing viruses. We observed excitatory, monosynaptic projections from layer 5 of the ipsilateral insula, targeting both PV interneurons and projection neurons in the claustrum with similar connection

(C) Examples of co-labeling of claustrum neurons in ACC-frontal (RSP) ACC-sensorimotor cortices (AUD) and sensorimotor-sensorimotor projecting conditions (ACC-VIS).
(D) Percentage of co-labeled neurons as a proportion of green labeled neurons observed, the difference observed was not due to chance $p < 0.001$ (chi-square test).
(E) In the sensorimotor-sensorimotor condition, the percentage of co-labeled neurons as a proportion of green labeled neurons observed was not different between groups suggesting that the difference observed due to chance $p > 0.1$ (chi-square test).
(F) Percentage of co-localization was pooled for ACC-Frontal, ACC-sensorimotor and Sensorimotor-Sensorimotor conditions and chi-square test for the difference in co-localization showed that the difference in co-localization was significant $p < 0.001$ (chi-square test).
See Figure S6.

Please cite this article in press as: Chia et al., Synaptic Connectivity between the Cortex and Claustrum Is Organized into Functional Modules, Current Biology (2020), https://doi.org/10.1016/j.cub.2020.05.031

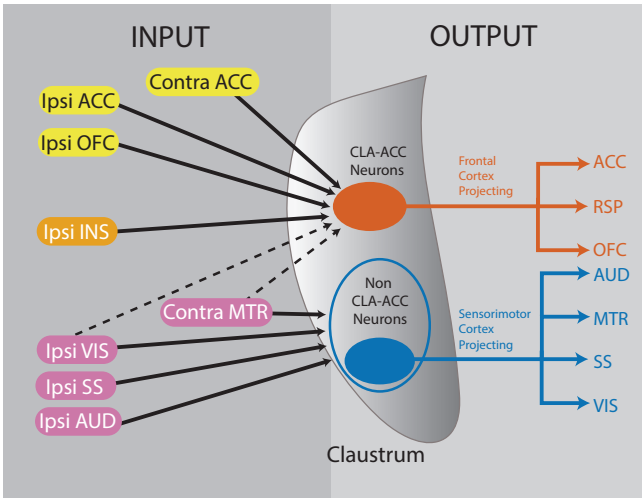

Figure 6. Modular Organization of Cortico-claustral Interconnectivity

A summary scheme of cortico-claustral interconnectivity. Cortical inputs from frontal and limbic regions (yellow and orange, respectively) show strong connection probability (solid line arrow) to CLA-ACC neurons while inputs from sensorimotor regions (purple) show either low connection probability (dashed line arrow) or no connection (no arrow). ACC-projecting claustrum neurons that receive preferential input from frontal and limbic cortices also preferentially co-project to other frontal cortices (orange). Another population of sensorimotor cortex targeting claustrum projection neurons was observed suggesting the existence of a sensorimotor cortex modality (blue). Abbreviations as follows: OFC, orbitofrontal cortex; ACC, anterior cingulate cortex; RSP, retrosplenial cortex; INS, insula; MTR, contralateral motor cortex; SS, somatosensory cortex; VIS, visual cortex; AUD, auditory cortex.

probabilities. PV interneurons have shorter response latency and larger EPSP size than projection neurons. This is in line with previous findings by Kim and colleagues [46], who studied sensorimotor input to the claustrum and proposed feedforward inhibition in the cortico-claustrum pathway. Excitatory input from the cortex targets both projection neurons and PV interneurons; projection neurons are then rapidly silenced through feedforward inhibition by PV interneurons within the claustrum circuity [5, 46]. This implies that a large input is required to depolarize claustrum projection neurons to fire within a small time-window in order for downstream synaptic propagation to occur. This mechanism is also observed in thalamocortical and corticostriatal pathways [64–67]. Collectively, limbic, sensory, [46] and frontal [12] cortical input to the claustrum suggests a general feedforward inhibitory circuit mechanism could be involved in the claustral processing of cortical inputs.

Feedforward inhibition [46] may support the idea of the claustrum as a coincidence detector [11] of salient or novel information [5, 68]. It narrows the time window for integration by curtailing excitatory responses and shortening the postsynaptic membrane time constant [64, 69–72]. Specifically, only stimuli from several cortical regions arriving at the claustrum within a short time window will activate claustrum projection neurons. They could, in turn, lead to a net inhibition of the cortical target [14]. Studies using all-optical interrogation methods [73, 74] support such a temporal convergence mechanism [75].

Claustrum Has at Least Two Distinct Cortical Targeting Systems

Stimulated by the fact that CLA-ACC neurons receive selective sets of inputs, we asked whether CLA-ACC neurons co-project to other cortical regions. We showed that CLA-ACC neurons co-labeled consistently with other frontal and limbic regions such as OFC and RSP, but that the same CLA-ACC population rarely co-labeled with sensorimotor regions (SS, AUD, VIS, MTR). We subsequently showed that a CLA-sensorimotor targeting system also existed, which was only sparsely connected to the frontal regions. Taken together, these data argue that claustrum projection neurons have at least two distinct targeting systems: one to frontal cortex and one to sensorimotor cortex (Figure 6). The use of retrograde tracers with higher false negative rates may account for the differences between our work and Zingg and colleagues [44], leading to an undercount of CLA-ACC neurons that co-project to sensorimotor areas. Full reconstructions of single cell neurons by Wang and colleagues [50] support our conclusion: we propose that the population of claustrum neurons projecting to frontal areas represents the CLA-I population described by Wang et al. [50], while the population of claustrum neurons projecting to sensorimotor areas represent the CLA-II population of Wang et al. [50].

CONCLUSION

Our results show that claustrum neurons projecting to the ACC receive direct input from certain cortical regions and not from others. This suggests a possible general organizational principle for the claustrum, where subpopulations of claustrum neurons are interconnected with selected cortical regions to form functional modules. Furthermore, we have identified a disynaptic circuit between insula, claustrum, and ACC, which could serve as the link connecting the principal nodes of the Salience Network. Finally, using an anatomical tracing method, we reveal that claustrum projection neurons are organized into at least two distinct targeting systems, frontal and sensorimotor. Collectively, our data suggest that the claustro-cortical pathways are organized into functional modules that could be specialized for processing different types of information.

STAR★METHODS

Detailed methods are provided in the online version of this paper and include the following:

- KEY RESOURCES TABLE
- RESOURCE AVAILABILITY
  - Lead Contact
  - Materials Availability
  - Data and Code Availability
- EXPERIMENTAL MODEL AND SUBJECT DETAILS
- METHOD DETAILS
  - Surgery
  - Brain slice preparation
  - Whole-cell patch clamp recordings
  - Claustrum identification
  - Photostimulation

- Confocal imaging
- Co-labeled CLA-ACC neurons

- QUANTIFICATION AND STATISTICAL ANALYSIS

SUPPLEMENTAL INFORMATION

Supplemental Information can be found online at https://doi.org/10.1016/j.cub.2020.05.031.

ACKNOWLEDGMENTS

We thank E. Dahlberg, M. Abbaszadeh, and A. Tokarska for technical assistance, M. Graf, A. Nair, G. Ham, M. Ketzef, M. Dorst, Y. Johansson, and R. de la Torre Martinez for helpful discussions. This work was supported by the Knut and Alice Wallenberg Foundation (KAW 2014.0051), The European Research Council (ERC 282012), The Swedish Brain Foundation (Hjärnfonden FO2018-0107), The Swedish Medical Research Council (VR-M 2015-02403), Karolinska Institute Strategic Progam for Neuroscience (StratNeuro), and grants from Karolinska Institutet, and a Singapore Ministry of Education (MOE2015-T2-2-095) grant to G.J.A. Z.C. was supported by the Nanyang Technological University - Karolinska Institutet Joint PhD Programme.

AUTHOR CONTRIBUTIONS

Z.C was responsible for experimental work and data analysis. G.S. administered the project. All authors were responsible for experimental design and manuscript writing.

DECLARATION OF INTERESTS

The authors declare no conflicts of interest.

Received: December 19, 2019
Revised: March 24, 2020
Accepted: May 7, 2020
Published: June 11, 2020

REFERENCES

1. Crick, F.C., and Koch, C. (2005). What is the function of the claustrum? Philos, R. Soc, ed. (B Biol. Sci), pp. 1271–1279.
2. Mathur, B.N. (2014). The claustrum in review. Front. Syst. Neurosci. *8*, 48.
3. Goll, Y., Atlan, G., and Citri, A. (2015). Attention: the claustrum. Trends Neurosci. *38*, 486–495.
4. Atlan, G., Terem, A., Peretz-Rivlin, N., Sehrawat, K., Gonzales, B.J., Pozner, G., Tasaka, G.I., Goll, Y., Refaeli, R., Zviran, O., et al. (2018). The claustrum supports resilience to distraction. Curr. Biol. *28*, 2752–2762.e7.
5. Remedios, R., Logothetis, N.K., and Kayser, C. (2010). Unimodal responses prevail within the multisensory claustrum. J. Neurosci. *30*, 12902–12907.
6. Patru, M.C., and Reser, D.H. (2015). A New Perspective on Delusional States - Evidence for Claustrum Involvement. Front. Psychiatry *6*. Published online November 9, 2015. https://doi.org/10.3389/fpsyt.2015.00158.
7. Chia, Z., Silberberg, G., and Augustine, G.J. (2017). Functional properties, topological organization and sexual dimorphism of claustrum neurons projecting to anterior cingulate cortex. Claustrum *2*. Published online August 23, 2017. https://doi.org/10.1080/20023294.2017.1357412.
8. Kitanishi, T., and Matsuo, N. (2017). Organization of the claustrum-to-entorhinal cortical connection in mice. J. Neurosci *37*, 269–280.
9. Edelstein, L.R., and Denaro, F.J. (2004). The claustrum: a historical review of its anatomy, physiology, cytochemistry and functional significance. Cell. Mol. Biol. *50*, 675–702.
10. Rahman, F.E., and Baizer, J.S. (2007). Neurochemically defined cell types in the claustrum of the cat. Brain Res. *1159*, 94–111.
11. Smythies, J., Edelstein, L., and Ramachandran, V. (2012). Hypotheses relating to the function of the claustrum. Front. Integr. Nuerosci. *6*. Published online August 2, 2012. https://doi.org/10.3389/fnint.2012.00053.
12. White, M.G., Panicker, M., Mu, C., Carter, A.M., Roberts, B.M., Dharmasri, P.A., and Mathur, B.N. (2018). Anterior Cingulate Cortex Input to the Claustrum Is Required for Top-Down Action Control. Cell Rep. *22*, 84–95.
13. Ptito, M., and Lassonde, M.C. (1981). Effects of claustral stimulation on the properties of visual cortex neurons in the cat. Exp. Neurol. *73*, 315–320.
14. Jackson, J., Karnani, M.M., Zemelman, B.V., Burdakov, D., and Lee, A.K. (2018). Inhibitory Control of Prefrontal Cortex by the Claustrum. Neuron *99*, 1029–1039.e4.
15. Tsumoto, T., and Suda, K. (1982). Effects of stimulation of the dorsocaudal claustrum on activities of striate cortex neurons in the cat. Brain Res. *240*, 345–349.
16. Spector, I., Hassmannova, Y., and Albe-Fessard, D. (1970). A macrophysiological study of functional organization of the claustrum. Exp. Neurol. *29*, 31–51.
17. Li, Z.K., Takada, M., and Hattori, T. (1986). Topographic organization and collateralization of claustrocortical projections in the rat. Brain Res. Bull. *17*, 529–532.
18. Clarey, J.C., and Irvine, D.R. (1986). Auditory response properties of neurons in the claustrum and putamen of the cat. Exp. Brain Res. *61*, 432–437.
19. Olson, C.R.R., and Graybiel, A.M. (1980). Sensory maps in the claustrum of the cat. Nature *288*, 479–481.
20. Smith, J.B., Radhakrishnan, H., and Alloway, K.D. (2012). Rat claustrum coordinates but does not integrate somatosensory and motor cortical information. J. Neurosci. *32*, 8583–8588.
21. Zhang, X., Hannesson, D.K., Saucier, D.M., Wallace, A.E., Howland, J., and Corcoran, M.E. (2001). Susceptibility to kindling and neuronal connections of the anterior claustrum. J. Neurosci. *21*, 3674–3687.
22. Zingg, B., Hintiryan, H., Gou, L., Song, M.Y., Bay, M., Bienkowski, M.S., Foster, N.N., Yamashita, S., Bowman, I., Toga, A.W., and Dong, H.W. (2014). Neural networks of the mouse neocortex. Cell *156*, 1096–1111.
23. Torgerson, C.M., and Van Horn, J.D. (2014). A case study in connectomics: the history, mapping, and connectivity of the claustrum. Front. Neuroinform. *8*, 83.
24. White, M.G., Cody, P.A., Bubser, M., Wang, H.D., Deutch, A.Y., and Mathur, B.N. (2016). Cortical hierarchy governs rat claustrocortical circuit organization. J. Comp. Neurol. *525*, 1347–1362.
25. Atlan, G., Terem, A., Peretz-Rivlin, N., Groysman, M., and Citri, A. (2017). Mapping synaptic cortico-claustral connectivity in the mouse. J. Comp. Neurol. *525*, 1381–1402.
26. Bush, G., Luu, P., and Posner, M.I. (2000). Cognitive and emotional influences in anterior cingulate cortex. Trends Cogn. Sci. *4*, 215–222.
27. Shenhav, A., Botvinick, M.M., and Cohen, J.D. (2013). The expected value of control: an integrative theory of anterior cingulate cortex function. Neuron *79*, 217–240.
28. Heilbronner, S.R., and Hayden, B.Y. (2016). Dorsal Anterior Cingulate Cortex : A Bottom-Up View. Annu. Rev. Neurosci. *8*, 149–170.
29. Seeley, W.W., Menon, V., Schatzberg, A.F., Keller, J., Glover, G.H., Kenna, H., Reiss, A.L., and Greicius, M.D. (2007). Dissociable intrinsic connectivity networks for salience processing and executive control. J. Neurosci. *27*, 2349–2356.
30. Sridharan, D., Levitin, D.J., and Menon, V. (2008). A critical role for the right fronto-insular cortex in switching between central-executive and default-mode networks. Proc. Natl. Acad. Sci. USA *105*, 12569–12574.
31. Medford, N., and Critchley, H.D. (2010). Conjoint activity of anterior insular and anterior cingulate cortex: awareness and response. Brain Struct. Funct. *214*, 535–549.

32. Menon, V., and Uddin, L.Q. (2010). Saliency, switching, attention and control: a network model of insula function. Brain Struct. Funct. *214*, 655–667.
33. Sforazzini, F., Schwarz, A.J., Galbusera, A., Bifone, A., and Gozzi, A. (2014). Distributed BOLD and CBV-weighted resting-state networks in the mouse brain. Neuroimage *87*, 403–415.
34. Mechling, A.E., Hübner, N.S., Lee, H.L., Hennig, J., von Elverfeldt, D., and Harsan, L.A. (2014). Fine-grained mapping of mouse brain functional connectivity with resting-state fMRI. Neuroimage *96*, 203–215.
35. Liska, A., Galbusera, A., Schwarz, A.J., and Gozzi, A. (2015). Functional connectivity hubs of the mouse brain. Neuroimage *115*, 281–291.
36. Pagani, M., Bifone, A., and Gozzi, A. (2016). Structural covariance networks in the mouse brain. Neuroimage *129*, 55–63.
37. White, M.G., and Mathur, B.N. (2018). Frontal cortical control of posterior sensory and association cortices through the claustrum. Brain Struct. Funct. *223*, 2999–3006.
38. Petreanu, L., Mao, T., Sternson, S.M., and Svoboda, K. (2009). The subcellular organization of neocortical excitatory connections. Nature *457*, 1142–1145.
39. Klapoetke, N.C., Murata, Y., Kim, S.S., Pulver, S.R., Birdsey-Benson, A., Cho, Y.K., Morimoto, T.K., Chuong, A.S., Carpenter, E.J., Tian, Z., et al. (2014). Independent optical excitation of distinct neural populations. Nat. Methods *11*, 338–346.
40. Johansson, Y., and Silberberg, G. (2020). The Functional Organization of Cortical and Thalamic Inputs onto Five Types of Striatal Neurons Is Determined by Source and Target Cell Identities. Cell Rep. *30*, 1178–1194.e3.
41. Wang, Q., Ng, L., Harris, J.A., Feng, D., Li, Y., Royall, J.J., Oh, S.W., Bernard, A., Sunkin, S.M., Koch, C., and Zeng, H. (2017). Organization of the connections between claustrum and cortex in the mouse. J. Comp. Neurol. *525*, 1317–1346.
42. Narikiyo, K., Mizuguchi, R., Ajima, A., Mitsui, S., Shiozaki, M., Hamanaka, H., Johansen, J.P., Mori, K., and Yoshihara, Y. (2018). The Claustrum Coordinates Cortical Slow-Wave Activity. bioRxiv, 286773.
43. Smith, J.B., Watson, G.D.R., Liang, Z., Liu, Y., Zhang, N., and Alloway, K.D. (2019). A Role for the Claustrum in Salience Processing? Front. Neuroanat. *13*. Published online June 19, 2019. https://doi.org/10.3389/fnana.2019.00064.
44. Zingg, B., Dong, H.W., Tao, H.W., and Zhang, L.I. (2018). Input-output organization of the mouse claustrum. J. Comp. Neurol. *526*, 2428–2443.
45. Real, M.Á., Dávila, J.C., and Guirado, S. (2003). Expression of calcium-binding proteins in the mouse claustrum. J. Chem. Neuroanat. *25*, 151–160.
46. Kim, J., Matney, C.J., Roth, R.H., Brown, S.P., and Brown, S.P. (2016). Synaptic Organization of the Neuronal Circuits of the Claustrum. J. Neurosci. *36*, 773–784.
47. Minciacchi, D., Molinari, M., Bentivoglio, M., and Macchi, G. (1985). The organization of the ipsi- and contralateral claustrocortical system in rat with notes on the bilateral claustrocortical projections in cat. Neuroscience *16*, 557–576.
48. Smith, J.B., and Alloway, K.D. (2014). Interhemispheric claustral circuits coordinate sensory and motor cortical areas that regulate exploratory behaviors. Front. Syst. Neurosci. *8*, 93.
49. Ollerenshaw, D., Shelton, A., Davis, J., Wang, Y., Zeng, H., Olsen, S.R., and Koch, C. (2018). Functional interrogation of claustrum involvement in a visual change detection task. In Proceedings of 48th Annual Meeting of the Society for Neuroscience, 306.07 / GG8.
50. Wang, Y., Xie, P., Gong, H., Zhou, Z., Kuang, X., Wang, Y., et al. (2019). Complete single neuron reconstruction reveals morphological diversity in molecularly defined claustral and cortical neuron types. bioRxiv. https://doi.org/10.1101/675280.
51. Katz, L.C., Burkhalter, A., and Dreyer, W.J. (1984). Fluorescent latex microspheres as a retrograde neuronal marker for in vivo and in vitro studies of visual cortex. Nature *310*, 498–500.
52. Katz, L.C., and Iarovici, D.M. (1990). Green fluorescent latex microspheres: a new retrograde tracer. Neuroscience *34*, 511–520.
53. Vercelli, A., Repici, M., Garbossa, D., and Grimaldi, A. (2000). Recent techniques for tracing pathways in the central nervous system of developing and adult mammals. Brain Res. Bull. *51*, 11–28.
54. Fioravante, D., and Regehr, W.G. (2011). Short-term forms of presynaptic plasticity. Curr. Opin. Neurobiol. *21*, 269–274.
55. Galandra, C., Basso, G., Manera, M., Crespi, C., Giorgi, I., Vittadini, G., Poggi, P., and Canessa, N. (2018). Salience network structural integrity predicts executive impairment in alcohol use disorders. Sci. Rep. *8*. Published online September 27, 2018. https://doi.org/10.1038/s41598-018-32828-x.
56. White, T.P., Joseph, V., Francis, S.T., and Liddle, P.F. (2010). Aberrant salience network (bilateral insula and anterior cingulate cortex) connectivity during information processing in schizophrenia. Schizophr. Res. *123*, 105–115.
57. Palaniyappan, L., Mallikarjun, P., Joseph, V., White, T.P., and Liddle, P.F. (2011). Reality distortion is related to the structure of the salience network in schizophrenia. Psychol. Med. *41*, 1701–1708.
58. Manoliu, A., Riedl, V., Zherdin, A., Mühlau, M., Schwerthöffer, D., Scherr, M., Peters, H., Zimmer, C., Förstl, H., Bäuml, J., et al. (2014). Aberrant dependence of default mode/central executive network interactions on anterior insular salience network activity in schizophrenia. Schizophr. Bull. *40*, 428–437.
59. Qadir, H., Krimmel, S.R., Mu, C., Poulopoulos, A., Seminowicz, D.A., and Mathur, B.N. (2018). Structural Connectivity of the Anterior Cingulate Cortex, Claustrum, and the Anterior Insula of the Mouse. Front. Neuroanat. *12*, 100.
60. Craig, A.D. (2002). How do you feel? Interoception: the sense of the physiological condition of the body. Nat. Rev. Neurosci. *3*, 655–666.
61. Craig, A.D.B. (2009). How do you feel–now? The anterior insula and human awareness. Nat. Rev. Neurosci. *10*, 59–70 http://www.nature.com/articles/nrn2555.
62. Mesulam, M.M., and Mufson, E.J. (1982). Insula of the old world monkey. III: Efferent cortical output and comments on function. J. Comp. Neurol. *212*, 38–52.
63. Mufson, E.J., and Mesulam, M.-M. (1982). Insula of the old world monkey. II: Afferent cortical input and comments on the claustrum. J. Comp. Neurol. *212*, 23–37.
64. Cruikshank, S.J., Lewis, T.J., and Connors, B.W. (2007). Synaptic basis for intense thalamocortical activation of feedforward inhibitory cells in neocortex. Nat. Neurosci. *10*, 462–468.
65. Reig, R., and Silberberg, G. (2014). Multisensory integration in the mouse striatum. Neuron *83*, 1200–1212.
66. Delevich, K., Tucciarone, J., Huang, Z.J., and Li, B. (2015). The mediodorsal thalamus drives feedforward inhibition in the anterior cingulate cortex via parvalbumin interneurons. J. Neurosci. *35*, 5743–5753.
67. Silberberg, G., and Bolam, J.P. (2015). Local and afferent synaptic pathways in the striatal microcircuitry. Curr. Opin. Neurobiol. *33*, 182–187.
68. Remedios, R., Logothetis, N.K., and Kayser, C. (2014). A role of the claustrum in auditory scene analysis by reflecting sensory change. Front. Syst. Neurosci. *8*. Published online April 4, 2014. https://doi.org/10.3389/fnsys.2014.00044.
69. König, P., Engel, A.K., and Singer, W. (1996). Integrator or coincidence detector? The role of the cortical neuron revisited. Trends Neurosci. *19*, 130–137.
70. Pouille, F., and Scanziani, M. (2001). Enforcement of temporal fidelity in pyramidal cells by somatic feed-forward inhibition. Science *293*, 1159–1163.
71. Wehr, M., and Zador, A.M. (2003). Balance inhibition underlies tuning and sharpens spike timing in auditory cortex. (Supplementary material). Nature *426*, 442–446.

72. Gabernet, L., Jadhav, S.P., Feldman, D.E., Carandini, M., and Scanziani, M. (2005). Somatosensory integration controlled by dynamic thalamocortical feed-forward inhibition. Neuron *48*, 315–327.

73. Packer, A.M., Roska, B., and Häusser, M. (2013). Targeting neurons and photons for optogenetics. Nat. Neurosci. *16*, 805–815.

74. Packer, A.M., Russell, L.E., Dalgleish, H.W.P., and Häusser, M. (2015). Simultaneous all-optical manipulation and recording of neural circuit activity with cellular resolution in vivo. Nat. Methods *12*, 140–146.

75. Packer, A.M., Yuan, T., Pettit, N., Chun, S., Lau, J.Y.N., and Häusser, M. (2015). Integration of multisensory inputs by single neurons in the claustrum. In 45th Society for Neuroscience Annual Meeting (Chicago, IL, USA: 2015 Neuroscience Meeting Planner), 788.16/M7.

76. Lee, J.H., Durand, R., Gradinaru, V., Zhang, F., Goshen, I., Kim, D.S., Fenno, L.E., Ramakrishnan, C., and Deisseroth, K. (2010). Global and local fMRI signals driven by neurons defined optogenetically by type and wiring. Nature *465*, 788–792.

77. Boyden, E.S., Zhang, F., Bamberg, E., Nagel, G., and Deisseroth, K. (2005). Millisecond-timescale, genetically targeted optical control of neural activity. Nat. Neurosci. *8*, 1263–1268.

78. Schneider, C.A., Rasband, W.S., and Eliceiri, K.W. (2012). NIH Image to ImageJ: 25 years of image analysis. Nat. Methods *9*, 671–675.

79. Hippenmeyer, S., Vrieseling, E., Sigrist, M., Portmann, T., Laengle, C., Ladle, D.R., and Arber, S. (2005). A developmental switch in the response of DRG neurons to ETS transcription factor signaling. PLoS Biol. *3*, e159.

80. Madisen, L., Zwingman, T.A., Sunkin, S.M., Oh, S.W., Zariwala, H.A., Gu, H., Ng, L.L., Palmiter, R.D., Hawrylycz, M.J., Jones, A.R., et al. (2010). A robust and high-throughput Cre reporting and characterization system for the whole mouse brain. Nat. Neurosci. *13*, 133–140.

81. Berry, M.S., and Pentreath, V.W. (1976). Criteria for distinguishing between monosynaptic and polysynaptic transmission. Brain Res. *105*, 1–20.

82. Doyle, M.W., and Andresen, M.C. (2001). Reliability of monosynaptic sensory transmission in brain stem neurons in vitro. J. Neurophysiol. *85*, 2213–2223.

83. Susaki, E.A., Tainaka, K., Perrin, D., Kishino, F., Tawara, T., Watanabe, T.M., Yokoyama, C., Onoe, H., Eguchi, M., Yamaguchi, S., et al. (2014). Whole-brain imaging with single-cell resolution using chemical cocktails and computational analysis. Cell *157*, 726–739.

84. Susaki, E.A., Tainaka, K., Perrin, D., Yukinaga, H., Kuno, A., and Ueda, H.R. (2015). Advanced CUBIC protocols for whole-brain and whole-body clearing and imaging. Nat. Protoc. *10*, 1709–1727.

85. Fuzik, J., Zeisel, A., Máté, Z., Calvigioni, D., Yanagawa, Y., Szabó, G., Linnarsson, S., and Harkany, T. (2015). Integration of electrophysiological recordings with single-cell RNA-seq data identifies neuronal subtypes. Nat. Biotechnol. *34*, 175–183.

Please cite this article in press as: Chia et al., Synaptic Connectivity between the Cortex and Claustrum Is Organized into Functional Modules, Current Biology (2020), https://doi.org/10.1016/j.cub.2020.05.031

STAR★METHODS

KEY RESOURCES TABLE

REAGENT or RESOURCE	SOURCE	IDENTIFIER
Antibodies		
Cy™5 AffiniPure Donkey Anti-Rabbit IgG (H+L)	Jackson ImmunoResearch Laboratories	RRID: AB_2340607
Bacterial and Virus Strains		
pAAV2-CaMKIIa-hChR2(H134R)-EYFP	[76]	Addgene 26969
pAAVrg-Syn-ChR2(H134R)-GFP	[77]	Addgene 58880
Chemicals, Peptides, and Recombinant Proteins		
Isoflurane, Forene	AbbVie AB (Apoteket)	Cat#506949
Sodium pentobarbital	APL	Cat#338327
Temgesic	Indivior Europe Limited (Apoteket)	Cat#521634
D-APV	Tocris	#0106; CAS; 79055-68-8
NBQX disodium salt	Tocris	#1044; CAS; 479347-86-9
Tetrodoxin citrate (TTX)	Tocris	#1069; CAS; 18660-81-6
4-Aminopyridine	Tocris	#0940; CAS; 504-24-5
SR-95531 (Gabazine)	Sigma-Aldrich	#S106; CAS; 104104-50-9
Experimental Models: Organisms/Strains		
Mouse, PV-Cre	Jackson Laboratory	RRID: IMSR_JAX: 017320
Mouse, Ai9 (RCL-tdT)	Jackson Laboratory	RRID: IMSR_JAX: 007909
Mouse, C57BL/6J	Jackson Laboratory	RRID: IMSR_JAX: 000664
Software and Algorithms		
IGOR Pro 6.37	Wavemetrics	http://www.wavemetrics.com
Graphpad	Graphpad	http://www.graphpad.com
ImageJ	[78]	https://imagej.nih.gov/ij/
ZEN Blue 2.3	Carl Zeiss	https://zeiss.com

RESOURCE AVAILABILITY

Lead Contact

Any further information and requests should be directed to and will be fulfilled by the Lead Contact, Gilad Silberberg (gilad.silberberg@ki.se).

Materials Availability

This study did not generate new unique reagents.

Data and Code Availability

The dataset and codes supporting the current study have not been deposited in a public repository because of their size and non-standard format but they are available from the Lead Contact upon request.

EXPERIMENTAL MODEL AND SUBJECT DETAILS

All experiments were performed according to the Guidelines of the Stockholm municipal committee for animal experiments. 38 adult C56/BL6J (RRID: IMSR_JAX: 000664) mice of both sexes were used to study multi-cortical input to CLA-ACC neurons (Figure 1-3). 31 adult PV-tdTomato mice were used to study the nature of insula input to the claustrum (Figure 4); these mice were from C57/BL6 background and were bred internally by crossing PV-Cre mice [79] (RRID: IMSR_JAX: 017320) with tdTomato reporter mouse line [80] (RRID: IMSR_JAX: 007909). 41 adult C56/BL6J mice of both sexes were used to investigate co-labeling of projections (Figure 5). Mice were at least one month old before surgery.

Please cite this article in press as: Chia et al., Synaptic Connectivity between the Cortex and Claustrum Is Organized into Functional Modules, Current Biology (2020), https://doi.org/10.1016/j.cub.2020.05.031

METHOD DETAILS

Surgery

Mice were anesthetized with isoflurane and placed in a stereotaxic frame (Harvard Apparatus). To investigate multi-cortical input to CLA-ACC neurons, two small craniotomies were made during the same surgery. The first craniotomy targeted the ACC with retrograde fluorescent beads while the second craniotomy targeted different cortical sites with anterograde ChR2 virus. To maximize transport efficiency of the retrograde beads, aliquots of beads were sonicated for 10 min prior to surgery. To target the ACC, a craniotomy was made to target 0.7 mm anterior to Bregma, 0.2 mm lateral to the midline and 1.4 mm ventral according to the Paxinos and Franklin Mouse Atlas, coordinates were individually adjusted according to the mouse brain measured by Bregma-Lambda distance with 0-point located at cranial level. 250 nL of red retrograde beads (250 nl; Lumafluor, Durham, NC, USA) were delivered at a rate of 100 nL/min. To target different cortical sites between 100 – 400 nL of virus (AAV2-CaMKIIa-hChR2(H134R)-EYFP, Addgene 26969; Penn Vector Core, Philadelphia, PA, USA) was injected by a micropipette using Quintessential Stereotaxic Injector (Stoelting Europe, Dublin, Ireland). The pipette was held in place for 3-5 min after the injection before being slowly retracted from the brain. To optimize comparisons across mice, the following steps were taken: 1) mice were all between 2-3 months old at time of injection, 2) mice of both sexes were used to determine whether responses were found in both sexes, 3) In order to normalize viral expression across cortical regions, different volumes of virus were injected based on the cortical region examined. These injection protocols are detailed in the table below.

Injection protocol for multi-cortical projection investigation.

To study sensorimotor cortical input to non CLA-ACC cells, 3 mice were injected with the ChR2 into both ipsilateral visual and auditory cortices and 2 mice were injected with ChR2 into both the somatosensory and contralateral motor cortices. To study insula input to the claustrum, a small craniotomy window was made to target virus injection to the insula. The coordinates used were adjusted according to each animal to correspond with the following coordinates on the Paxinos and Franklin Mouse Atlas: 0.7 mm anterior to bregma, 2.9 mm lateral to the midline and 3.75 mm. 100 nL of anterograde ChR2 virus (AAV2-CaMKIIa-hChR2(H134R)-EYFP, Addgene 26969; Penn Vector Core, Philadelphia, PA, USA) was delivered at a rate of 200 nL/min, these coordinates would target layer 5 of the insula. To target layer 2/3 of the insula the injection site was moved 3.1 mm to the midline. The pipette was held in place for 3 min after the injection before being slowly retracted from the brain. Post-injection analgesics were given (0.03 mg/kg buprenorphine). An injection was deemed successful if visual inspection of slices showed that the injection avoided the PV-rich core and around 50 μm of the putative shell region.

To investigate co-labeling of projection neurons, red retrograde beads and green beads were injected into different cortical regions at the speed of 100 nL/min and a volume of 300 nL per craniotomy, up to three craniotomies per cortical region were made. The pipette was held in place for 5 min after the injection before being slowly retracted from the brain. The specific injection protocols are detailed in the table below.

Injection protocol and cell counts for co-labeling of projection neurons.

Retrograde Bead Injection Parameters								Cell Counts		
	Red Beads			Green Beads			Number	Red Beads	Green	Co-
Cortical Site (Red-Green)	L-M	A-P	D-V	L-M	A-P	D-V	of Mice	Only	Beads Only	labeled
ACC-Auditory Cortex	−0.3	1.2	−1.6	−3.6	−1.9	−2	4	523	67	10
	−0.3	0.5	−1.3	−3.7	−2.7	−2.5				
				−3.8	−3.4	−2.5				
ACC-Visual Cortex	−0.3	1.2	−1.6	−2.4	−2.1	−1.2	5	798	145	25
	−0.3	0.5	−1.3	−3	−2.8	−1.3				
				−2.5	−3.5	−1.3				
ACC-Somatosensory Cortex	−0.3	1.2	−1.6	−3.2	0.5	−2.2	6	718	121	13
	−0.3	0.5	−1.3	−2.7	−0.4	−1.5				
ACC-Motor Cortex	−0.3	1.2	−1.6	−1.3	1.8	−1.1	5	830	295	45
	−0.3	0.5	−1.3	−1.1	1.1	−1.1				
ACC-Retrosplenial Cortex	−0.3	1.2	−1.6	−0.3	−1.3	−1.2	5	990	116	130
	−0.3	0.5	−1.3	−0.2	−1.8	−0.7				
ACC- Orbitofrontal Cortex	−0.3	1.2	−1.6	−1	2.8	−2.5	6	813	78	65
	−0.3	0.5	−1.3	−1	2.2	−2.7				

(*Continued on next page*)

Continued

Retrograde Bead Injection Parameters								Cell Counts		
	Red Beads			Green Beads			Number	Red Beads	Green	Co-
Cortical Site (Red-Green)	L-M	A-P	D-V	L-M	A-P	D-V	of Mice	Only	Beads Only	labeled
Auditory-Visual	−3.6	−1.9	−2.1	−2.4	−2.1	−1.2	3	355	59	34
	−3.7	−2.7	−1.6	−3	−2.8	−1.3				
	−3.9	−3.4	−2.5	−2.5	−3.5	−1.3				
Auditory-Somatosensory	−3.6	−1.9	−2	−3	1.2	−2.3	4	285	71	27
	−3.7	−2.7	−2.5	−3.1	0.5	−2.5				
	−3.9	−3.4	−2.5	−3	−0.6	−1.5				
Motor-Somatosensory	−1.5	2	−1.6	−3	1.2	−2.3	3	365	97	39
	−1.5	1.2	−1.6	−3.1	0.5	−2.5				
	−1.2	0.5	−1.4	−3	−0.6	−1.5				

Brain slice preparation

Mice were sacrificed at least 20 days following injections and used for slice recordings. Mice were anesthetized with isoflurane and their brains removed in ice-cold cutting solution containing the following (in mM): 2.5 KCl, 1.25 NaH_2PO_4, 0.5 $CaCl_2$, 7.5 $MgCl_2$, 10 glucose, 25 $NaHCO_3$, 205 sucrose. Coronal slices, 250 μm thick, were cut (Leica VT 1000S, Wetzlar, Germany), then transferred to a 35°C water bath for one h in artificial CSF containing the following (in mM): 125 NaCl, 25 glucose, 25 $NaHCO_3$, 2.5 KCl, 2 $CaCl_2$, 1.25 NaH_2PO_4, 1 $MgCl_2$. Slices were subsequently removed from the water bath and kept at room temperature (22 – 24°C). Slices were subsequently transferred for experiments into a bath artificial CSF solution with 10 μM of gabazine and were kept for no longer than 10 h after the brain was sliced.

Whole-cell patch clamp recordings

Whole-cell patch recordings were obtained at 35 ± 0.5°C. Glass electrodes were pulled with a micropipette puller (P-97, Sutter Instruments) and had resistances of 7–9 MΩ. They contained (in mM) 130 K-gluconate, 5 KCl, 10 HEPES, 4 Mg-ATP, 0.3 Na-GTP, 10 Na_2-phosphocreatine and in some experiments 0.3% Neurobiotin. Neurons were visualized with infrared differential interference contrast (IR-DIC) microscopy (Zeiss FS Axioskop) and fluorescent microscopy, using a mercury lamp (HBO 100, Zeiss) and a fluorescent filter cube mounted on the same microscope. Pairs of neurons were recorded within a range of 100 μm between somata. Recordings were amplified using MultiClamp 700B (Molecular Devices) and digitized by an ITC-18 (HEKA Elektronik) acquisition board. Data were acquired and analyzed using IGOR Pro (WaveMetrics). Responses with latencies longer than 5 ms or temporal jitter standard deviation larger than 0.5 ms [81, 82] were assumed to be polysynaptic and therefore were excluded from statistical analysis. An additional method used for distinguishing between monosynaptic and polysynaptic responses was the bath application of tetrodotoxin (TTX, 1 μM) and 4-Aminopyridine (4AP, 100 μM), as previously described [38].

Claustrum identification

In experiments in which adult C56/BL6J mice were used, the claustrum was identified by retrograde beads injected into the ACC. Such retrograde bead labeling was previously shown [7] to localize in the claustrum core and were used therefore to identify the claustrum. Where PV transgenic mice were used, the claustrum was identified via the enriched neuropil region between the striatum and insula.

Photostimulation

Photostimuli were generated by a blue LED (1 Watt power, 465 nm wavelength) mounted on the microscope oculars and delivered through the objective lens. Photostimulation was controlled by a LED driver (Mightex Systems) connected to the ITC-18 acquisition board, enabling control of light flash duration and intensity. The maximal light power as measured directly under the objective lens was 1.35 mW. Unless otherwise stated, light intensity was roughly 50% of the maximal value. Short light flashes (2 ms duration, 8 pulses at 10 Hz, followed by a single 2 ms light flash after another 500 ms) were delivered to evoke postsynaptic responses in neurons; these responses were recorded with the patch pipette. Light trains were repeated at least 20 times, at 10 s intervals; responses were considered to arise from a ChR2-expressing synaptic input if the response occurred at a consistent time after photostimulation.

Confocal imaging

In some experiments, slices used for whole-cell patch recording were fixed in Lana's fixative (4% PFC with picric acid) to image the cortical injection sites for post hoc confirmation. Slices were fixed overnight and subsequently washed in PBS 6 times, for 10 min each wash. Slices were then mounted on a glass slide with 70% glycerol and DABCO mounting medium. In cases where the experiment included 0.3% Neurobiotin, slices incubated in Cy5 (1:1000 with PBS) for at least 72 h prior mounting on a slide. Confocal images were acquired using confocal microscopy (Zeiss LSM 510).

Co-labeled CLA-ACC neurons

To ensure that cell counting was robust and decrease false negative/positive rates, the injected mice were processed in two ways: thin cryostat slices and thick brain slices. Every experimental condition included at least one mouse processed by thin or thick methods. Mice used for thin cryostat slices received an overdose of sodium pentobarbital (200 mg/kg I.P.), and transcardially perfused with 4% PFA in 0.01M PBS. The brain was removed and kept for additional 2 h in the 4% PFA, after which it was transferred to 0.01M PBS. A day before sectioning, the brain was transferred to and kept in 12% sucrose solution in 0.01M PBS. Coronal slices of 16 μm cryo-sections were prepared from the region between 1.7 mm anterior to 1.2 mm posterior to bregma on a cryostat (Microm HM 560). Slices were subsequently mounted on gelatin coated microscope slides and imaged under a widefield fluorescence microscope (Olympus BX51), with 10x and 20x objectives and post processed on ImageJ software. Mice used for thick brain slice counting were anesthetized with isoflurane and their brains removed in ice-cold cutting solution containing the following (in mM): 2.5 KCl, 1.25 NaH2PO4, 0.5 CaCl2, 7.5 MgCl2, 10 glucose, 25 NaHCO3, 205 sucrose. Coronal slices, 350 μm thick, were cut (Leica VT 1000S, Wetzlar, Germany), fixed overnight in Lana's fixative (4% PFC with picric acid) and subsequently washed in PB 6 times, for 10 min each wash. Slices were cleared using "CUBIC Reagent 1" (25 wt% urea, 25 wt% N,N,N′,N′-tetrakis(2-hydroxypropyl) ethylenediamine and 15 wt% polyethylene glycol mono-p-isooctylphenyl ether/Triton X-100) overnight [83–85]. After 6 washes in PB for 10 min each wash. Slices were counter stained with 1:4000 DAPI: PB for 10 min. Slices were then rewashed in PB and submerged in "CUBIC Reagent 2" (50 wt% sucrose, 25 wt% urea, 10 wt% 2,20,20′-nitrilotriethanol and 0.1% v/v% Triton X-100) for further clearing and then mounted on gelatin coated microscope slides. Confocal images were acquired using confocal microscopy (Zeiss LSM 510, Stockholm, Sweden) using 10 and 20x objectives and analyzed using Carl Zeiss ZEN software. In both cases, a double-blind approach was taken in which the labeling of retrieved brains was coded and then randomized for the imaging session prior to manual cell counting.

QUANTIFICATION AND STATISTICAL ANALYSIS

All statistical analyses were performed in GraphPad Prism QuickCalcs Online and are reported together with the specific statistical test as well as the value and description of the number of recorded cells (n) in the figure legends. For parametric data, t test was performed after datasets passed the Shapiro-Wilk test for normality. Results are presented in the text as mean ± SEM. For non-parametric data, chi-square test were performed on the dataset, for small samples sizes ($n < 3$), Fishers Exact test Statistical significance is defined as * $p < 0.05$, ** $p < 0.01$, and *** $p < 0.001$, if not noted otherwise.